NMR studies of the most conserved RNA domain of the mammalian signal recognition particle (SRP)

U. Schmitz, D. M. Freymann, T. L. James, R. J. Keenan, R. Vinayak and P. Walter

RNA 1996 2: 1213-1227

RNA (1996), 2:1213–1227. Cambridge University Press. Printed in the USA.

NMR studies of the most conserved RNA domain of the mammalian Signal Recognition Particle (SRP)

ULI SCHMITZ,[1] DOUGLAS M. FREYMANN,[2] THOMAS L. JAMES,[1] ROBERT J. KEENAN,[2] RAVI VINAYAK,[3] and PETER WALTER[2]

[1] Department of Pharmaceutical Chemistry, University of California, San Francisco, California 94143-0446, USA
[2] Department of Biochemistry and Biophysics, University of California, San Francisco, California 94143-0448, USA
[3] Applied Biosystems, 850 Lincoln Centre Drive, Foster City, California 94404, USA

ABSTRACT

Mammalian signal recognition particle (SRP) and its homologues exhibit a phylogenetically conserved RNA domain, whose predicted secondary structure exhibits a hairpin motif with two bulged regions. Two RNA fragments comprising one (24 nt) or two (43 nt) of the conserved bulges were studied. Each fragment binds specifically to the domain of the *Escherichia coli* homologue of the SRP54 protein, which is involved in signal sequence recognition. The SRP RNA fragments exhibited a pronounced structural stabilization in the presence of Mg^{2+}. Assignments of all base, H1′, H2′, and most imino proton resonances in the presence of Mg^{2+} were obtained for the 24mer RNA via NOE spectroscopy and correlated homonuclear NMR methods. 2D NOE patterns permitted a coarse structural description, revealing a relatively compact A-type geometry for the 24mer without any indications of looped-out nucleotides, syn-oriented bases, or base triplets. The GGAA-loop is structurally very similar to that of the GCAA tetraloop [Heus HA, Pardi A, 1991, *Science 253*:191–194]. Mg^{2+} seems to stabilize the structure of the conserved bulged region, which involves G:A and C:A mismatch pairs. Deviations from ideal A-type helicity are found for a larger region than the predicted secondary structure implies. Although no explicit assignment effort has been dedicated to the 43mer yet, striking similarity in chemical shift changes upon addition of Mg^{2+} allowed some structural conclusions. The bulge present in both RNA fragments exhibits a similar, pronounced flexibility in the absence of Mg^{2+}, indicating that the additional bulge in the 43mer does not stabilize the other bulge.

Keywords: NMR of RNA; RNA–protein recognition; signal recognition particle

INTRODUCTION

Protein translocation across the membrane involves the interaction between ribosomes and the signal recognition particle. In the current view (Walter & Johnson, 1994; Lütcke, 1995), SRP recognizes a signal sequence in the nascent protein and binds tightly to the active ribosome. This in turn causes translational arrest, followed by the targeting of the dormant ribosome–SRP complex to the SRP receptor in the ER membrane.

Mammalian SRP is comprised of a 300-nt RNA and six distinct proteins (SRP 9, 14, 19, 54, 68, and 72) (Walter & Johnson, 1994). SRP RNA homologues have been found for a wide range of species and phylogenetic comparisons (Larsen & Zwieb, 1993; Althoff et al., 1994) suggest a conserved four-domain structure (Poritz et al., 1988). Domain IV exhibits the largest conservation of both sequence and secondary structure, suggestive of a key role for this region. Indeed, domain IV interacts with SRP54 (Walter & Johnson, 1994), which is also instrumental in recognizing the peptide signal sequence. SRP54 may be separated proteolytically into two well-defined domains: an N-terminal domain (34 kDa), which harbors GTPase activity, and a C-terminal domain (20 kDa), which contains both the RNA binding and the signal sequence binding sites (Römisch et al., 1990; Zopf et al., 1990, 1993; High

Reprint requests to: Uli Schmitz, Department of Pharmaceutical Chemistry, University of California, San Francisco, California 94143-0446, USA; e-mail schmitz@picasso.ucsf.edu.

Abbreviations: tRNA, transfer ribonucleic acid; $O.D._{260}$, optical density at 260 nm at 25 °C; MWCO, molecular weight cutoff; NOESY, NOE spectroscopy; TOCSY, total correlation spectroscopy; DQF-COSY, double quantum filtered correlation spectroscopy; T_m, UV-melting point; DMS, dimethylsulfate; DEPC, diethylpyrocarbonate; CMCT, 1-cyclohexyl-3-(-morpholinoethyl) carbodiimide methane-*p*-toluene sulfonate; ER, endoplasmic reticulum; TSP, trisilylpropionic acid sodium salt; fid, free induction decay; *ffh*, fifty-four-homologue; *ffhM*, methionine-rich domain of fifty-four-homologue; SRP, signal recognition particle.

et al., 1991). Because of its high content of methionine residues, the second domain was termed M-domain (Bernstein et al., 1989).

An SRP54 homologue was found in *Escherichia coli*, termed *ffh* (Bernstein et al., 1989; Römisch et al., 1989), that exhibits similarity in both sequence and domain structure. *Ffh* can replace mammalian SRP54 in signal sequence recognition when it is part of a chimeric particle (Bernstein et al., 1993). Also, mammalian SRP54 binds to *E. coli* 4.5S RNA, the *E. coli* SRP RNA homologue (Römisch et al., 1990; Zopf et al., 1990). Indeed, such a chimeric complex has been demonstrated to facilitate translocation of nascent protein (Hauser et al., 1995).

Some recent studies provide broad structural insights into the *ffh* interaction with 4.5S RNA. Lentzen et al. (1994) used enzymatic and chemical probing to elucidate RNA–protein contact points and suggested a bend located in the highly conserved RNA domain IV. Kurita et al. (1996) obtained a 91-amino acid *ffh* deletion mutant comprising only two of the three α-helical regions of *ffhM*, which binds as tightly to 4.5S RNA as intact *ffh*. However, a detailed structural understanding of the RNA–protein interaction as it relates to signal sequence recognition is only possible via high-resolution techniques. Although crystallization of RNA or RNA–protein complexes is still an unpredictable, painstaking endeavor, the application of NMR methods is limited mainly by the size of the molecules (Wüthrich, 1986; Wagner, 1993). However, heteronuclear NMR methods applied to ^{13}C, ^{15}N-labeled RNA (Nikonowicz & Pardi, 1993; Pardi, 1995) have pushed the applicability of NMR to a molecular size of more than 40 nt. Also, modern spectral processing techniques have pushed the size of RNAs to be studied with homonuclear NMR to more than 20 nt (Borer et al., 1995).

Our goal is the determination of the solution structure of the *ffhM*–domain IV complex, which is capable of recognizing signal sequences. The present paper describes preliminary structural studies of SRP RNA fragments from different parts of domain IV. Our RNA model is comprised of 43 nt containing both of the conserved bulged regions of the hairpin motif, depicted in Figure 1. A 24-nt fragment was also synthesized, omitting the symmetric bulge and the end of domain IV. Both fragments bind tightly and specifically to *ffhM*.

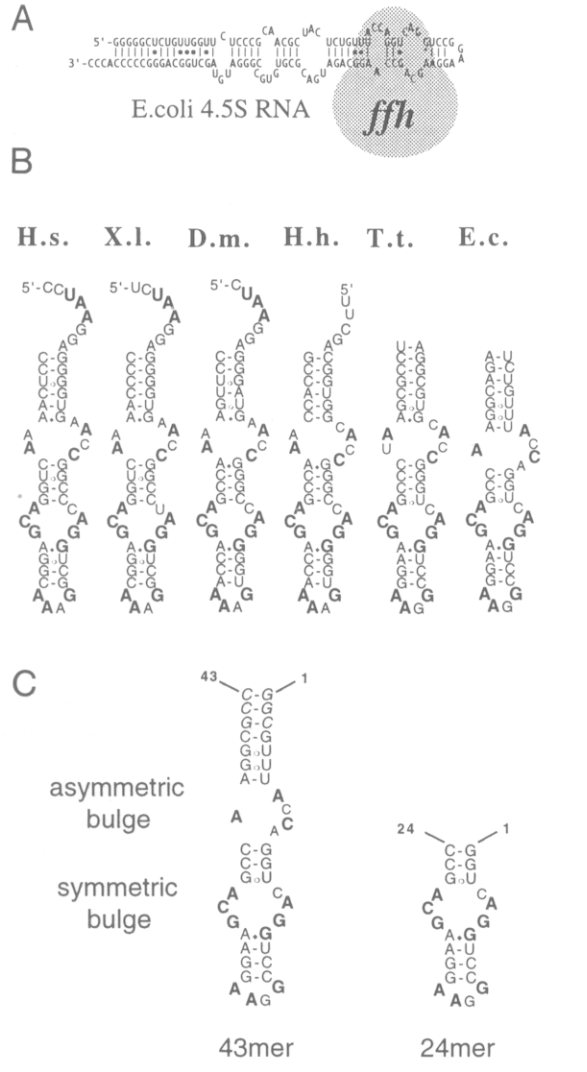

FIGURE 1. Predicted secondary structures for *E. coli* 4.5S RNA and domain IV sequences. **A:** 4.5S RNA and putative binding site for *ffh*. **B:** Conserved hairpin motif for domain IV of various species with phylogenetically conserved nucleotides (bold) (H.s., *Homo sapiens*; X.l., *Xenopus laevis*; D.m., *Drosophila melanogaster*; H.h., *Halobacterium halobium*; T.t., *Thermus thermophilus*; E.c., *E. coli*). **C:** Sequences of SRP RNA fragments for NMR studies.

RESULTS AND DISCUSSION

Sequence design

The conserved secondary structure for SRP RNA domain IV contains a distinct hairpin motif with two bulged regions separated by 3–4 base pairs. The apical moiety is generally closed by a GNRA-tetraloop, whose structural stability is believed to provide a unique nucleation site for folding (Woese et al., 1990; Heus & Pardi, 1991). Figure 1 depicts 4.5S RNA and domain IV secondary structure alignments for Eucarya, Archaea, and Bacteria. The phylogenetically conserved nucleotides all reside in the bulged regions and the tetraloop, suggesting that they play a critical role in the biological function. Note that even the putative stem regions exhibit a significant amount of non-Watson–Crick base pairs, especially in close proximity to the bulges; for example, the symmetric bulge is almost always flanked at the loop end by a putative G:A base pair.

For NMR analysis, we chose the slightly modified *E. coli* sequence shown in Figure 1C. Because we wanted to use in vitro transcription with T7 RNA polymerase to synthesize the NMR sample, the native 5′-UCU was

modified to 5′-GGC, containing the mandatory 5′-G and for reasons of better transcription yields. Chemical and enzymatic modification data of 4.5S RNA and the *ffh*–4.5S RNA complex (Lentzen et al., 1994) suggested that domain IV does not assume the rod-like shape suggested by the secondary structure analysis, but exhibits a bend that most likely occurs in the asymmetric bulge. It is possible to build models that use largely A-form geometries, where the two bulged regions are placed in close proximity to each other. The structure of the bulged regions and the relationship between them would be most informative to elucidate. As a first step, we constructed a 24-nt fragment of domain IV that does not have the asymmetric bulge. The advantage of analyzing this shorter fragment lies in the fact that proton resonance assignments can be obtained via homonuclear NMR with unlabeled material, whereas the 43-nt fragment requires a heteronuclear approach using ^{13}C- and/or ^{15}N-labeled samples. We expect that results determined with the 24mer will be helpful for the NMR work with the 43mer. For example, the asymmetric bulge in the 43mer does not contain additional imino protons, which might lead to quick structural insights regarding the symmetric bulge in the 43mer by simple comparison of the imino proton spectra. Other NMR features of the 24mer might be recognizable in the 43mer spectra as well. This approach should address the context-dependence of NMR structures of RNA fragments. We should be able to determine whether the structure of the symmetric bulge changes when it is taken out of the context of the complete domain IV.

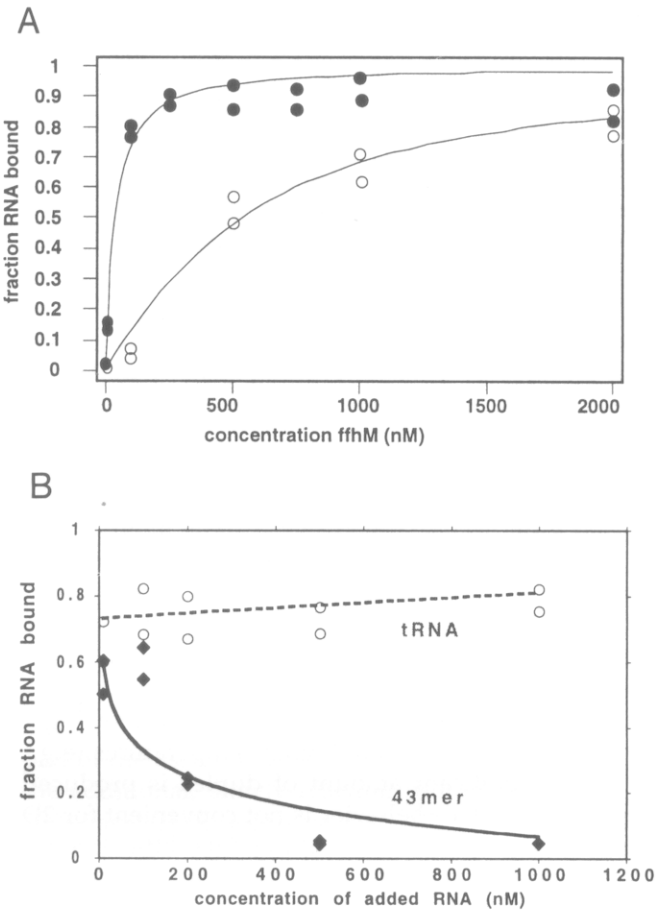

FIGURE 2. RNA retention curves from nitrocellulose filter binding. **A:** Titration of SRP RNA fragments with *ffhM*, 43mer in 10 mM Mg^{2+} (●); 24mer in 10 mM Mg^{2+} (○). Lines represent best fit for general binding equation. **B:** Competition binding titration of 24mer with tRNA (○; two independent data sets shown) and 43mer (◆; two independent data sets shown) (for experimental detail, see text).

Binding studies

Before embarking on structural studies, it is crucial to verify the biological significance of the construct. Therefore, we determined the equilibrium constant of complex formation with *ffhM* utilizing nitrocellulose filter binding assays (Jones & Berg, 1966). The binding affinity of full *ffh* for 4.5.S RNA has been reported to be in the nanomolar range ($K_D \leq 300$ nM [Lentzen et al., 1994; Kurita et al., 1996]). For the present work, we have assayed RNA binding to *ffhM* under conditions that could be used for NMR samples, i.e., reducing additional salts to a minimum. As depicted in Figure 2A, the 43mer binds more tightly to *ffhM* (5–50 nM) than the 24mer (300–600 nM), which indicates that the asymmetric bulge must contribute significantly to the binding. Both complexes were subjected to competition binding experiments to ascertain the specificity of the complex formation (Fig. 2B). For both of our complexes, neither tRNA nor the smaller, more flexible T-arm of tRNA (Yao et al., 1996), could compete with assembly of the *ffhM*–SRP RNA complex.

Mg^{2+} and presumably other salts play an important role in stabilizing mammalian SRP (Walter & Johnson, 1994). However, in our binding assays, we found that neither Na^+ nor Mg^{2+} concentrations affected the apparent *ffhM*–RNA binding affinity; using Na^+ concentrations up to 500 mM and omitting Mg^{2+}, which is typically present in SRP related assays, does not interfere with tight binding (data not shown). The latter results are surprising, given our structural results from NMR and UV melting (see below), which revealed a pronounced Mg^{2+} effect on structure and stability. Obviously, *ffhM* finds recognition elements in the RNA for both conditions, with and without Mg^{2+}. Regarding the fact that some of the protein–RNA interactions in mammalian SRP involve divalent cations, our results preclude that Mg^{2+} is involved in mediating *ffhM* domain IV interactions.

Thermodynamic measurements and RNA hairpin stability

Usually, RNA hairpin stability is demonstrated by the independence of the melting point, T_m, from the RNA

concentration (Puglisi & Tinoco, 1989). However, this procedure cannot indicate the presence of mixtures unequivocally, and the T_m concentration effects grow smaller with the size of the RNA being studied. In our UV melting studies, neither the 43mer nor the 24mer exhibited concentration-dependent melting over a range from 0.8 to 48 μM RNA (see Fig. 3A). However, 1D NMR studies revealed quickly that both RNA samples contained two species, in varying ratios, depending on salt conditions and annealing protocols. Size-exclusion chromatography (Puglisi & Wyatt, 1995), which enables an easy calibration of the molecular weight, verified the NMR results. Both sequences, but especially the shorter one, form a dimeric species, whose presence increases with time, addition of salt ([NaCl] 20–500 mM; [$MgCl_2$] 1–5 mM), and when the sample is allowed to cool slowly overnight after heating. (The molecular weight for duplex and hairpin species was verified with analytical ultracentrifugation for the SRP 43mer.) In general, duplex-free solutions can be obtained via snap-cooling of a buffered RNA solution and subsequent addition of salts after cooling. However, when the 24mer hairpin, stabilized by Mg^{2+} (1–5 mM), is incubated at higher temperatures (e.g., 50 °C), a significant amount of duplex is produced within hours. This behavior is not convenient for 2D NMR studies, and makes melting data difficult to interpret as at higher temperatures duplex might be present as well.

With respect to the thermodynamic stability of the two RNA fragments, a pronounced T_m increase is produced by the addition of Mg^{2+}. For the 24mer, Mg^{2+} or Na^+ (>100 mM) is required to form pure hairpin. In low-salt buffers (10 mM potassium cacodylate), the 24mer exists as a hairpin–duplex mixture, indicated by gel filtration studies, and exhibits a broad transition around 46 °C and a sharper transition at 64 °C (Fig. 3A). However, upon addition of 5 mM $MgCl_2$ after snap-cooling, only one sharp transition at 69 °C is observed, reflecting the hairpin melting. The increased hypochromicity at higher RNA concentrations must be attributed to RNA aggregation effects. The Mg^{2+}-induced stabilization for the 43mer is even more striking, as Figure 3B shows (T_m = 44 °C in 10 mM potassium cacodylate versus T_m = 78 °C with addition of 10 mM $MgCl_2$). Our results suggest that the stabilization is Mg^{2+}-specific, because neither large Na^+ concentrations nor Ca^{2+}, the divalent cation most similar to Mg^{2+}, can provide the stabilization effect of Mg^{2+} (e.g., T_m = 68 °C for 500 mM NaCl; T_m = 69 °C for 1 mM $CaCl_2$ versus T_m = 76 °C for 1 mM $MgCl_2$).

According to Laing et al. (1994), melting data alone can be used to discriminate between specific and non-specific Mg^{2+} binding. Among other things, it was shown that the presence of an Mg^{2+}-specific binding site should lead to a plot of $1/T_m$ versus ln [Mg^{2+}] that is linear up to high Mg^{2+} concentrations. In the case of the 24mer, low Mg^{2+} concentrations rendered melting curves with broad, not readily assignable transitions. For the 43mer, however, one well-defined hairpin melting transition was found for all Mg^{2+}-concentrations, leading to a $1/T_m$ versus ln [Mg^{2+}] profile shown

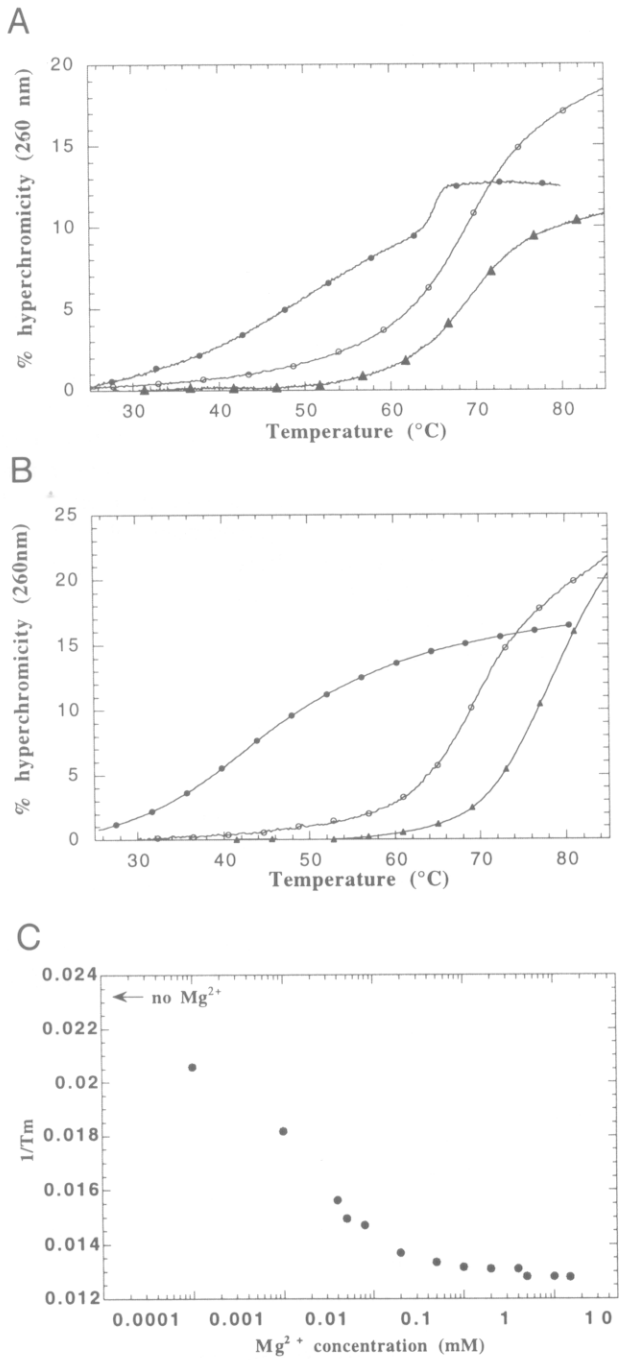

FIGURE 3. UV melting analysis of SRP RNA fragments. **A:** Melting profiles of 24mer in 10 mM potassium cacodylate, pH 6.5, [RNA] 0.8 μM (●); with addition of 10 mM $MgCl_2$ (▲); with addition of 10 mM $MgCl_2$ and [RNA] 48 μM (○). **B:** Melting profiles of 43mer in 10 mM potassium cacodylate, pH 6.5, [RNA] 1 μM (●); with addition of 10 mM $MgCl_2$ (▲); with addition of 1 mM $CaCl_2$ (○); **C:** Dependence of T_m upon Mg^{2+} concentration for 43mer in 10 mM potassium cacodylate, pH 6.5, [RNA] 1 μM.

in Figure 3C. The 43mer data are linear up to 0.1 mM and level off at higher concentrations. Although the single 43mer melting point probably encompasses more than one discrete transition, our UV data, in conjunction with our NMR results, suggest the presence of a specific Mg^{2+} site in addition to the common Mg^{2+}-induced stabilization of double helices.

NMR studies

As expected from UV and gel filtration results, 1D NMR spectra of the 24mer change significantly when the Mg^{2+} concentration is raised to 10 mM. Furthermore, comparison of 2D NOE spectra obtained with and without Mg^{2+} showed that the 24mer is more structured in the presence of Mg^{2+}, indicated by a larger number of NOE crosspeaks. Unfortunately, high Mg^{2+} concentrations also lead to severe broadening of the proton resonances due to RNA aggregation. Only the combination of slightly elevated temperatures (25 °C, 30 °C, and 35 °C) and a very low RNA concentration (0.25 mM) enabled us to obtain 2D NMR data using a 10-mm homonuclear probe, sufficient for proton assignments in the presence of Mg^{2+}. In the following section, we will discuss the NMR work on the SRP 24mer, which will involve some comparisons with the 43mer, for which only a few assignments have been obtained to date.

Assignments of nonexchangeable protons

Our proton assignment strategy followed well-described methods utilizing largely 2D NOE data and homonuclear correlated experiments (DQF-COSY, TOCSY) (Varani & Tinoco, 1991; Wijmenga et al., 1994). However, the large number of unusual base pairings in conjunction with some unusually shifted proton resonances made our assignments anything but trivial. Because most of these unusual spectral features have structural implications, some comments on the assignment process are in order.

Resonance assignments of all base, H1′, and H2′ protons, and a number of H3′ and H4′ protons, could be accomplished utilizing 2D NOE data for various mixing times (50 ms, 150 ms, and 400 ms), temperatures, and Mg^{2+} concentrations (5 mM and 10 mM Mg^{2+}).

All eight pyrimidine base protons were identified readily in the correlated experiments by their H5–H6 crosspeaks. The intensity of one of the peaks was reduced significantly compared to the other ones, indicating local flexibility for residue C20. The region of the base protons exhibits the expected number of 30 resonances, including six adenine H2 protons. The latter usually can be identified by slower relaxation behavior. However, the partially relaxed 1D NMR spectra obtained with T_1 inversion recovery experiments exhibited an additional slowly relaxing proton. Complicating the matter, the typical region showing base → H1′ NOEs reveals only 21 H1′ resonances. Furthermore, no additional H1′ resonances could be identified from H1′ → H2′ contacts in the region of the H1′ → ribose proton NOE crosspeaks in 50-ms and 150-ms NOE data sets (spectra not shown).

The sequence of our 24mer loop is very similar to that of the GCAA-tetraloop, whose NMR structure has been solved previously (Heus & Pardi, 1991). One of the signatures of this tetraloop motif is the unusual upfield shift of the H1′ proton, which is situated under the baseplane of the guanine of the G:A closing base pair of the loop. Our NOE data exhibit the same peculiar feature ($\delta_{G15H1'} = 3.62$ ppm versus 3.65 ppm for the equivalent residue) found by Heus and Pardi (1991), which added an extra H1′ resonance and also provided an anchor point for the H1′ → H6/8 NOESY walk shown in Figure 4. A contiguous H1′ → H6/8 walk can be traced from residue G7 to A18. The intensity patterns are similar to that found for the GCAA tetraloop structure, i.e., weak sequential NOEs between G11 and G12, medium to strong NOEs for G12–A13 and A13–A14, plus a strong A13H2 → A14H1′ NOE. This part of the assignment also elucidated the identity of the additional, slowly relaxing proton as G12H8 (at 30 °C and 35 °C isochronous with A13H8). G12H8 might exhibit different relaxation properties because this residue was found to be disordered in the GCAA tetraloop structure. The other two stretches of the H1′ → H6/8 walk could be established unambiguously by relying on the purine–pyrimidine patterns in the sequence and adenine H2 → H1′ connectivities. Although it involved a number of very weak sequential NOEs, the G1–G6 stretch was straightforward. On the other hand, the G19–C24 trace left us short of the two H1′ assignments for the ends. As it turned out, the H1′ and the H2′ protons of C23 and C24 are completely overlapped and the H6 protons also have similar chemical shifts. Only the conspicuous intensity of the H1′ → H2′ NOE in the 50-ms NOESY and the intense H1′ → H2′ peak in the COSY spectra in the same location gave a clue that the typically flexible 3′-terminal residue's resonances, with its indicatively large $^3J_{H1'H2'}$ coupling constant and consequent COSY peak, and the C23 resonances are on top of each other. The last missing H1′ resonance, G19H1′, was eventually found with an unusual shift (4.72 ppm), although it does not exhibit any NOEs with H6 or H8 protons. In A-form helices, pyrimidine H5 protons usually exhibit sequential H5 → ribose proton NOEs, which were indeed found for C20. Adenine H2 protons are the only nonexchangeable protons that generally exhibit cross-strand connectivities, mostly involving H1′ protons. A strong NOE was observed for A5H2 and a ribose proton at 4.72 ppm (this frequency coincides with the solvent frequency in some of our spectra). Because we cannot necessarily assume regular A-form connectivities for the bulged re-

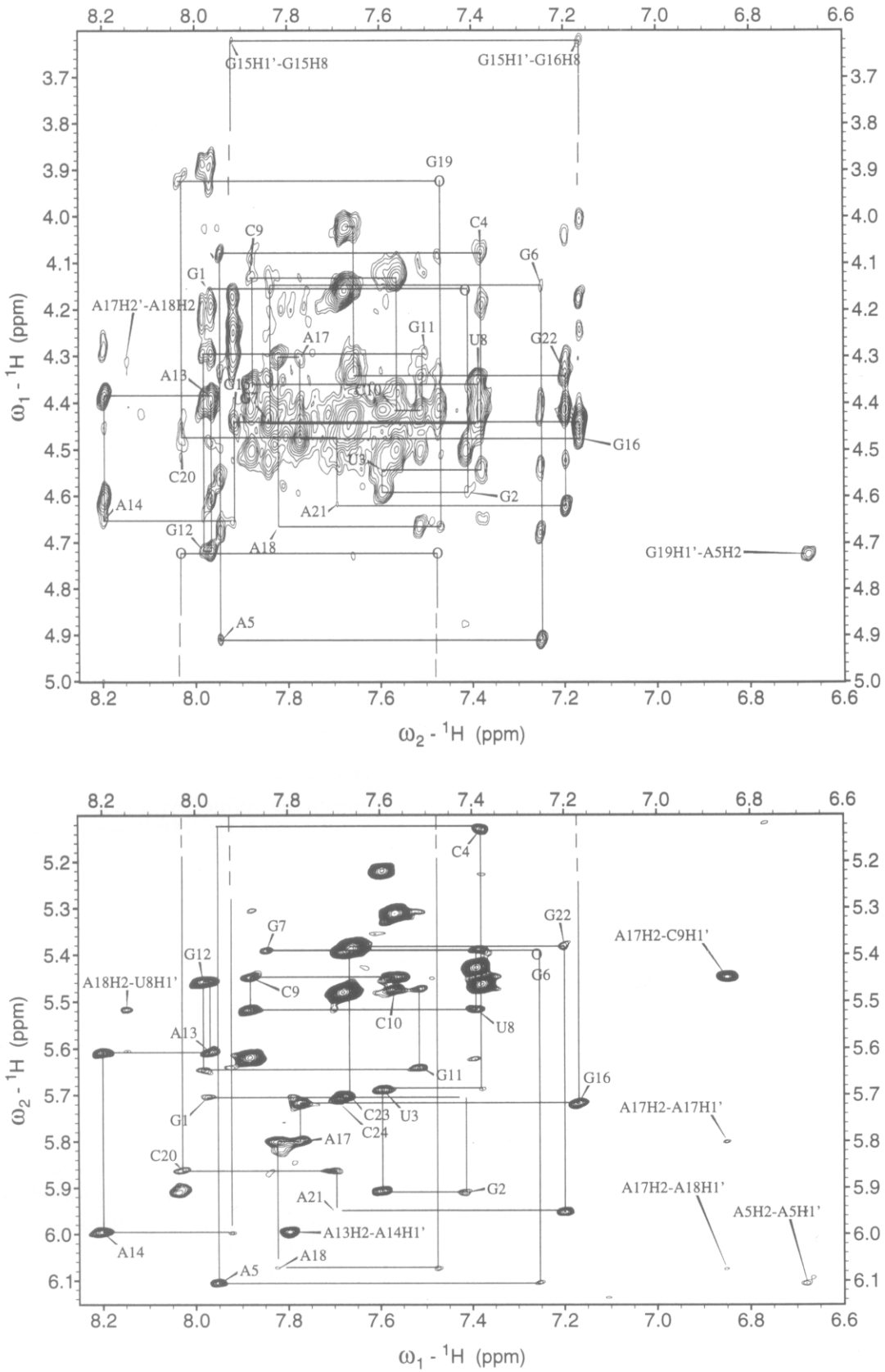

FIGURE 4. Sequential assignments for 24mer: (bottom) portion of the 400-ms 2D NOESY showing the base → H1′/H5 proton crosspeaks, and (top) portion with base → ribose proton crosspeaks. H6/8 → H1′ and H6/8 → H2′ NOESY walks are traced: the respective intraresidue peak is labeled with the residue number. Some instrumental peaks discussed in the text are labeled as well. For the situation where no peaks were observed in all spectra, the respective position is marked (○) to complete the walks.

gion, unambiguous assignment for that resonance to G19 H1′ comes from the observation that this proton has a strong crosspeak even in the 50-ms NOE data with the putative H2′-proton at 3.92 ppm, to which C20H5 shows a crosspeak.

An almost complete H2′→H6/8 NOESY walk could be traced despite severe overlap, lending confidence to our assignments (Fig. 4, top). Also, for all strong and medium sequential H1′→H6/8 NOEs, the equivalent sequential H1′→H2′ NOE was observed.

For the rest of the ribose protons, only partial assignments were obtained, mostly from analysis of correlated spectra and the H1′→ribose NOEs at low mixing times. Most of the H4′ assignments were obtained from weak H1′→ribose proton NOEs in the 50-ms NOE data, based on the assumption that, in the absence of spin diffusion, the H1′-H4′ crosspeak intensities should be larger than those for H1′-H3′. H3′ assignments were made when a weak H1′→ribose proton NOE that had not been assigned to H2′ or H4′ was found, for which a H6/8→ribose proton NOE of the same residue could also be found. This procedure bears the risk of confusing H3′ and H5′/5″ resonances and was therefore applied with modesty, yielding only a few unambiguous assignments.

Assignments for adenine H2 protons came from H2→H2 NOEs and from H2→H1′ NOEs, of which the cross-strand and sequential crosspeaks (e.g., A17H2→C9H1′, A18H2→U8H1′, and A17H2→A18H1′) yielded the absolute location in the sequence.

Although additional assignments could possibly be achieved using other homonuclear experiments, e.g., 2-quantum spectroscopy or edited NOESY-type experiments (Wijmenga et al., 1994), heteronuclear correlation data would be most helpful. Unfortunately, these data are difficult to come by with a natural abundance sample of 0.25 mM. We assume that the heteronuclear NMR work on the 43mer will ultimately augment the assignments for the 24mer protons.

Assignments of exchangeable protons

For the 12 nt in the 24mer with imino protons, only 10 resonances could be observed. 1D NMR spectra at different temperatures (5–30 °C) and Mg^{2+} concentrations (0–10 mM) (data not shown, but see Fig. 5A) indicated that the resonance cluster around 12.4 ppm involves four imino protons, of which only three could be assigned (G15, G16, and U3). Base pairs C10:G15 and C9:G16 are the most stable according to our temperature studies. The imino protons of the U3:G22 wobble pair were identified quickly through their unique chemical shifts ($\delta_{G22NH} = 10.56$; $\delta_{U3NH} = 12.35$) and the strong NH→NH NOE (Fig. 5, bottom). These two protons also exhibit an NOE with a common imino proton, which can only be G2NH. The 5′-terminal G1NH was assigned to 12.7 ppm on the basis of its

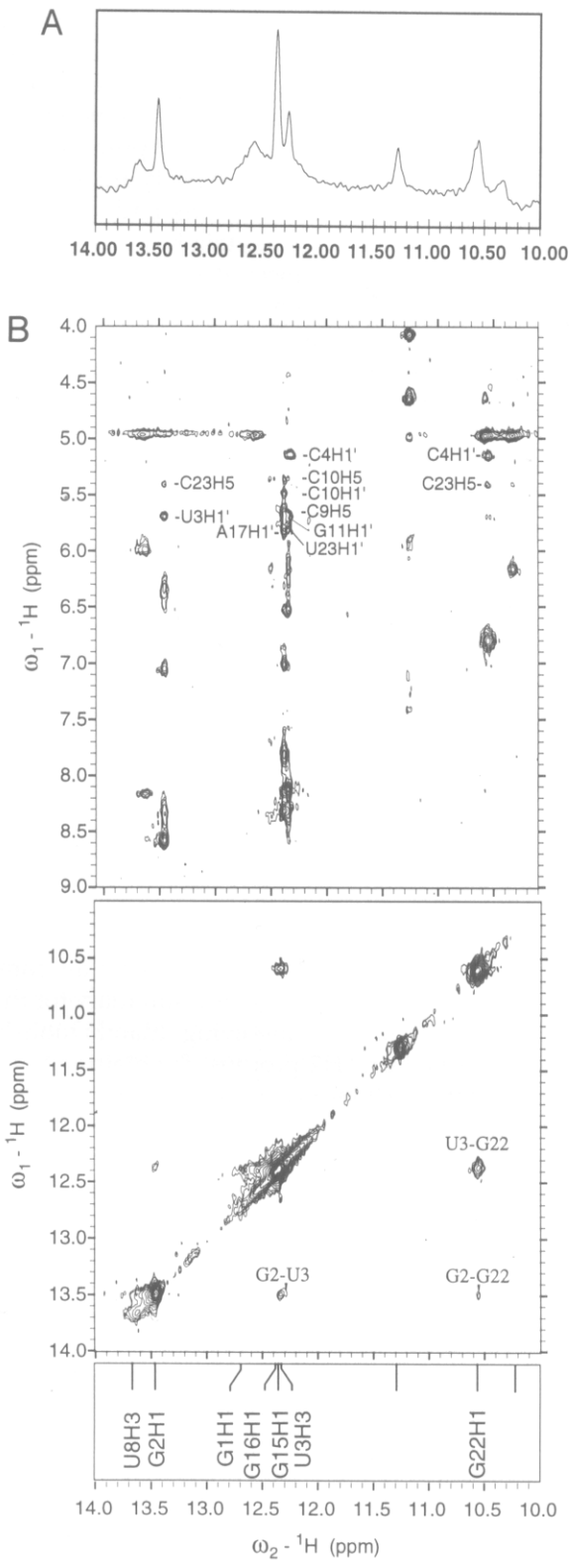

FIGURE 5. Portions of the 1D NMR and the 150-ms NOESY acquired in H_2O. **A:** Imino proton resonances of the 24mer (15 °C, 1.5 mM RNA, 7.5 mM $MgCl_2$, 10 mM potassium phosphate, pH 6.4). **B:** Imino proton NOE crosspeaks with other imino protons (bottom) and crosspeaks of imino→amino/H5/H1′ protons (top) (10 °C, 0.25 mM RNA, 5 mM $MgCl_2$, 10 mM potassium phosphate, pH 6.4). For the peak labels, the respective imino proton was not labeled; only unassigned crosspeaks or crosspeaks with amino protons are not labeled.

temperature dependence and chemical shift, although this resonance does not manifest NOEs to other residues. U8NH, which we expected to reveal itself readily through an NOE to A17H2, was assigned merely on the basis of chemical shift criteria (13.63 ppm). U8NH shows only two broad NOEs, most likely arising from the NOEs with A17 amino protons and not from A17H2. In the end, it was not certain how the remaining two broader NH resonances at 11.3 and 10.3 ppm could be assigned to the imino protons of G6, G7, G11, G12, and G19. Extrapolating from the GCAA tetraloop structure (Heus & Pardi, 1991), we would not expect to observe the imino resonance of a completely disordered residue (G12). Also, motivated by the spectral similarities for the loop region, we can assume a chemical shift for G11NH similar to that found for the equivalent position of the GCAA tetraloop (10.59 ppm [Heus & Pardi, 1991]), which would place G11NH at 10.35 ppm, or, alternatively, the signal at 10.56 ppm comprises two resonances. From the connectivities among the imino protons, it is clear that G6, G7, and G19 do not engage in base pairing that involves imino protons in strong hydrogen bonds. A final assignment for the NH resonance at 11.29 ppm will only come from assigning the protons at 4.63 and 4.07 ppm, to which it exhibits NOE crosspeaks.

Structural implications from qualitative NMR analysis

The chemical shift assignments for the 24mer are compiled in Table 1, and Figure 6 gives a summary for the observed sequential NOEs involving unambiguously assigned base, H1′, and H2′ protons. To obtain an NMR structure, NOEs are typically quantified and utilized in conformational search procedures. The number of unambiguously assigned interresidue NOEs (<5 per residue) and the unresolved imino proton assignments do not warrant high-resolution structure calculations for the 24mer. Nevertheless, our results offer ample information to devise a low-resolution model of the 24mer structure.

There are several indications that, under the conditions of low concentration (0.25 mM), presence of Mg^{2+}, and modest temperature (25 °C), the 24mer adopts a fairly stable structure that includes the bulged region: the H2′ → H6/8 NOESY walk can be traced around nearly the entire molecule; only two interruptions are found for the H1′ → H6/8 walk, both at the bulge-stem loop junction; furthermore, few sugar puckers deviate from typical A-form pucker (C3′-endo) and half of these deviations are found in the loop. Also, there are no hints for syn-orientation of bases, because no base → H1′ peaks are observed in NOE data with low mixing times. In light of these results, it is somewhat unexpected to see only a few direct indications of stable base pairings in the bulge region. From the

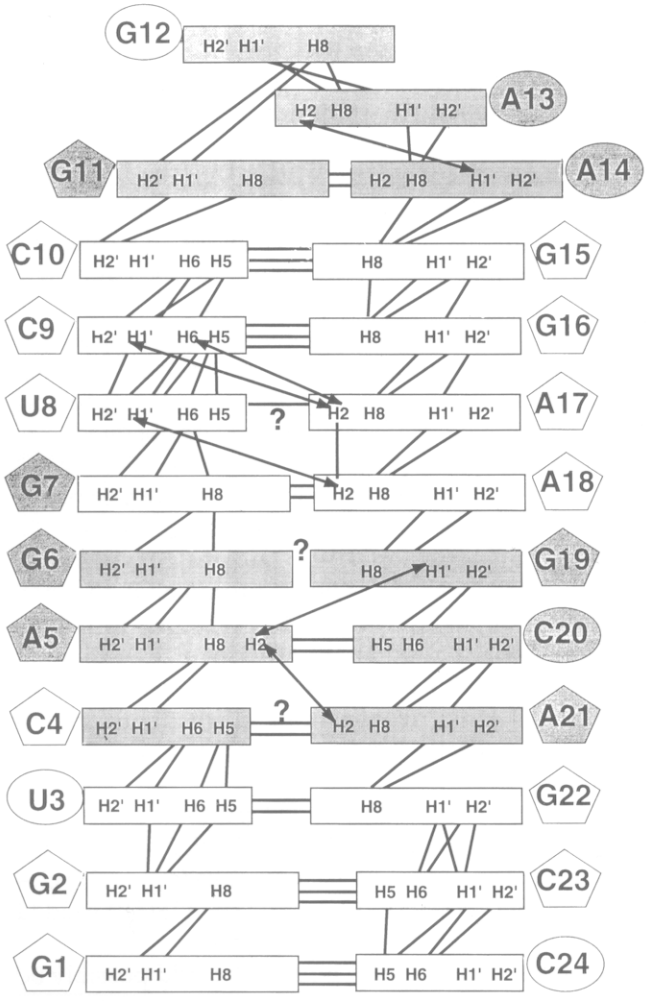

FIGURE 6. Summary of NOE connectivities of nonexchangeable protons for 24mer, based on several 400-ms 2D NOESY experiments. For orientation, base rectangles of loop and bulge residues are shaded. Phylogenetically conserved nucleotides are marked with shaded ribose symbol. The pentagon reflects C3′-endo ribose pucker, the oval reflects flexible or C2′-endo puckers. NOEs involving adenine H2 protons are shown as double-headed arrows. Question marks indicate that the form of base pairing was not completely identified; hydrogen bonds are depicted as horizontal lines between base rectangles.

NOE data obtained in H_2O, direct evidence for base pairing involving imino protons was found only for four base pairs (G2:C23, U3:G22, C9:G16, C10:G15). On the other hand, there are several base pairings in our SRP fragment that can be inferred. The most common form of G:A pairing involves amino protons, whose assignments are usually not available. For example, note that, in the case of the well-defined GCAA tetraloop structure (Heus & Pardi, 1991), the G:A base pair of the loop was not defined directly by NOEs, but was deduced by modeling a large number of NOEs involving nonexchangeable protons that assisted in positioning G and A baseplanes. In our case, the similarity of chemical shifts and NOE patterns relative to the GCAA tetraloop structure suggests a very similar structure for residues C9–G16. A simple picture can also be

TABLE 1. Proton chemical shift assignments for SRP 24mer (ppm) and $^3J_{H1'H2'}$ coupling constants (Hz).[a]

Residue	H8/H6	H5/H2	H1′	H2′	H3′	H4′	Imino	Amino	$^3J_{H1'H2'}$
G1	7.97	–	5.71	4.16	n/a	n/a	12.7br	n/a	3>
G2	7.42	–	5.91	4.59	(4.41)	n/a	13.47	8.35/6.32	3>
U3	7.59	5.22	5.69	4.54	n/a	4.42	12.33	–	3–5
C4	7.38	5.46	5.13	4.08	(4.18)	4.55	–	n/a	3>
A5	7.95	6.68	6.11	4.91	(4.67)	4.56	–	n/a	3>
G6	7.25	–	5.39	4.15	(4.54)	n/a	n/a	n/a	3>
G7	7.84	–	5.39	4.44	4.35	n/a	n/a	n/a	3>
U8	7.39	5.43	5.52	4.37	n/a	4.42	13.63	–	3>
C9	7.88	5.62	5.45	4.13	4.50	n/a	–	8.32/7.01	3>
C10	7.57	5.31	5.47	4.42	n/a	n/a	–	8.12/6.53	3>
G11	7.51	5.64	5.64	4.29	n/a	4.42	(10.65)	n/a	3>
G12	7.98	–	5.46	4.72	(4.36)	(4.05)	n/a	n/a	6–8
A13	7.97	7.80	5.61	4.38	(4.18)	4.29	–	n/a	4–6sh
A14	8.20	7.94	6.00	4.66	(4.08)	4.46	–	n/a	4–6
G15	7.92	–	3.62	4.44	4.25	4.17	12.35	?/6.20	3>
G16	7.17	–	5.72	4.48	(4.39)	n/a	12.38	7.81/5.70	3>
A17	7.77	6.85	5.80	4.31	n/a	4.46	–	8.19/5.99	3>
A18	7.82	8.15	6.07	4.67	n/a	4.51	–	n/a	3>
G19	7.48	–	4.72	3.92	n/a	n/a	n/a	n/a	3>
C20	8.04	5.91	5.86	4.49	n/a	4.53	–	n/a	4–6
A21	7.70	8.12	5.95	4.62	n/a	4.53	–	n/a	3>
G22	7.20	–	5.39	4.34	(4.04)	n/a	10.56	?/6.80	3>
C23	7.67	5.39	5.71	4.02	4.16	n/a	–	8.61/7.06	3>
C24	7.68	5.48	5.72	4.02	(4.40)	(4.18)	–	n/a	5–7sh

[a] 10 mM potassium phosphate, pH 6.5, 5 mM $MgCl_2$, 298K, 0.25 mM RNA. Parentheses indicate tentative assignments; sh, sharp; br, broad.

drawn for the bottom stem of the hairpin, for which all NOE connectivities are found to be typical for an A-form helix, including the expected imino proton NOEs.

Structural interpretation of the NMR data of the bulged region and base pairs G7:A18 and U8:A17 is far less straightforward. Important insights came from the observation of spectral changes when the Mg^{2+} concentration was changed. Figure 7 depicts the changes in the downfield region of the 24mer spectrum upon titration with $MgCl_2$. Adenine H2 line widths have been recognized previously as reporters for local flexibilities in nucleic acid structures (Schmitz et al., 1992; Kennedy et al., 1993; Lingbeck et al., 1996). Broad lines are typically interpreted as indications of dynamic processes on relatively slow time scales, e.g., milliseconds (Schmitz et al., 1992). Figure 7A shows that, for the 24mer, when [Mg^{2+}] is raised to 5 mM, the chemical shift dispersion improves and several peaks sharpen considerably, e.g., A17H2 at 6.85 ppm, giving rise to at least one new signal at 6.68 ppm belonging to A5H2. A21H2 is also broad, but shifts to 8.12 ppm with sharpening upon addition of Mg^{2+}. A similar titration with the SRP 43mer (Fig. 7B) revealed the same behavior for two resonances at the same chemical shifts (6.6 and 6.8 ppm), identified as adenine H2 protons through their long relaxation times. These data not only suggest the same proton assignments, but also a similar structure, and similar influence of Mg^{2+}.

Our results for the SRP RNA fragments suggest that the symmetric bulge, including the two adjacent base pairs, congeal into a more defined and thermodynamically stable structure in the presence of Mg^{2+} cations, as indicated by the sharpening of adenine H2 resonances, seen in Figure 7. In addition, H6 and H8 resonances shift noticeably in this Mg^{2+}-titration. Note that some changes are seen for the three upfield guanine H8 resonances, assigned to G6, G16, and G22, suggesting that a large part of the 24mer structure is influenced by Mg^{2+}.

For the bulge adenines A5 and A21, a stable structure could potentially involve C:A^+ base pairs with protonation of the adenine N1 atom. The pK_a of the N1 position in free AMP was determined to be 4.0 (Legault & Pardi, 1994). However, local pK_a values might increase when the site is part of a particular RNA structure and the associated negative electrostatic potential of a nucleic acid helix. For example, the pK_a of a particular adenine N1 in the catalytically active region of a lead-activated ribozyme is 6.5, measured by the pH dependence of the ^{13}C2 chemical shift (Legault & Pardi, 1994). An A^+:C base pair was also detected in an RNA hairpin by monitoring the pH dependence of the adenine H2 resonance: the originally sharp resonance broadened significantly when the pH was raised from 5.5 to 7.2 (Puglisi et al., 1990).

In our case, increasing the pH leads to a similar effect. The pH dependence of the 1D NMR spectrum of

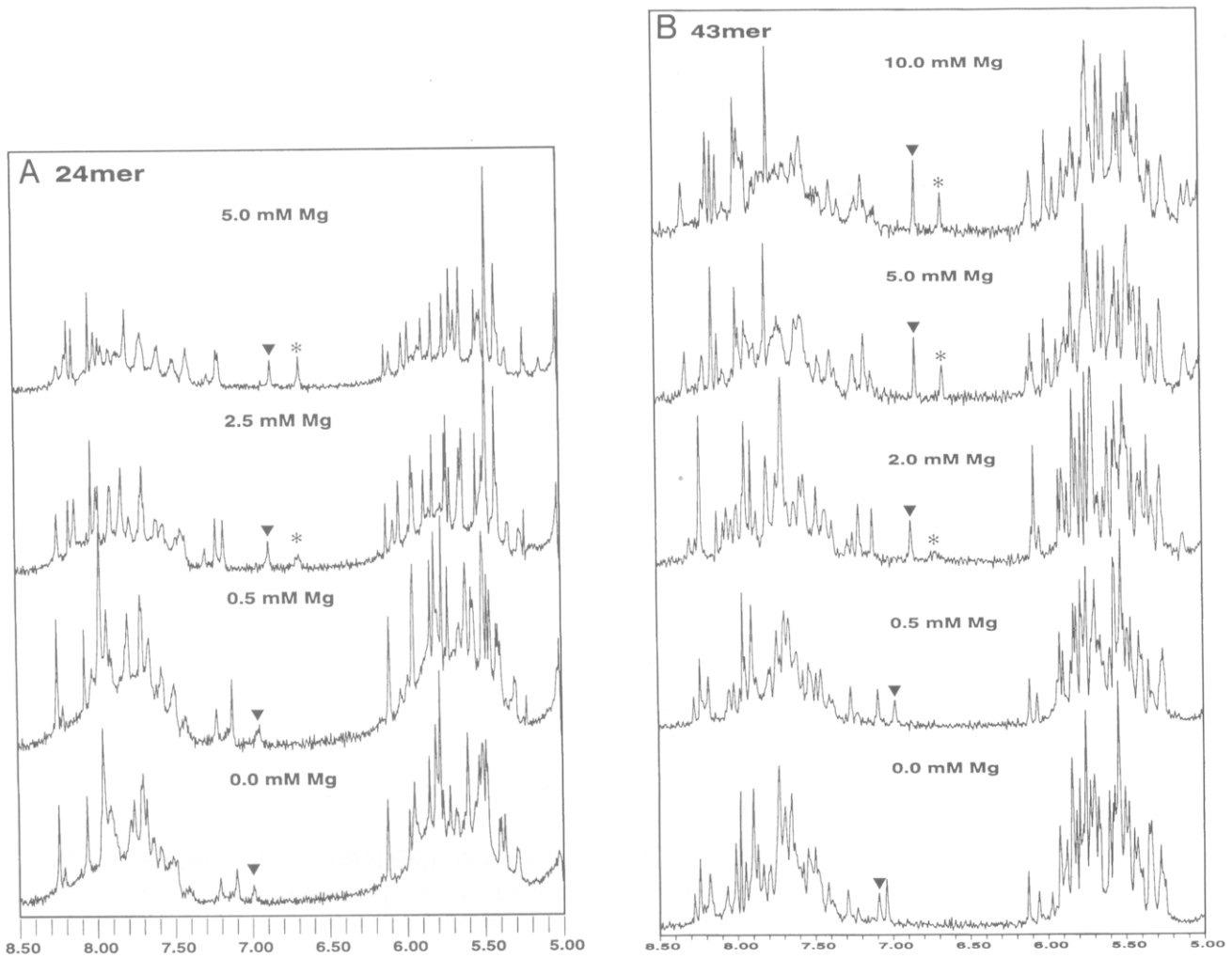

FIGURE 7. Titration of SRP RNA fragments with $MgCl_2$ (10 mM potassium phosphate, pH 6.5, 30 °C. Aromatic and anomeric region of ^1H NMR spectrum of (**A**) 24mer for various Mg^{2+} concentrations and (**B**) for 43mer. A17H2 (▼) and A5 H2 (*) resonances in the 24mer and the equivalent peaks in the 43mer resonances are marked.

the 24mer is shown in Figure 8, with the most striking changes above pH 8. The broadening of the A5H2 resonance at higher pH values is evident. Some changes can also be seen for the resonances around 8.13 ppm (A18H2 and A21H2); as the resonance at 8.15 ppm (A18H2) seems to loose its sharpness, we cannot be sure of its assignment at higher pH values because small chemical shift changes cannot be ignored. The broadening of the resonances at 7.20 and 7.25 ppm (G22H8 and G6H8) is also quite remarkable next to the unaffected G16H8 peak. Similarly, the two H1′ resonances that broaden with certainty are those of G6 and A18. These observations are consistent with the structure of the bulge becoming destabilized as the putative A^+:C base pairs fall apart.

The notion of a structured bulge is further supported by A5H2 connectivities to A21H1′ and G19H1′. The latter NOE is unusual for regular A-type geometries, which highlights the area around G6 and G19 as the most structurally deviant. Furthermore, missing sequential H1′ → H6/8 for steps G6pG7 and G19pC20, very weak sequential NOEs for A18pG19, and the absence of well-defined imino resonances for G6, G7, and G19 suggest a structural disruption for this end of the bulge. There is no direct evidence via observation of the G imino or amino proton resonances that the G7:A18 pair is actually formed, but we observe the NOEs that would place this base pair in a regular A-form helical stack, e.g., A17 and A18 bases should be stacked, because a medium-sized H2 → H2 NOE is seen. For G19, we have a strong indication that it is placed under A18 such that G19H1′ is exposed to the ring current effect of the A18 base, similar to the situation for G11:A14 and G15, which would explain the upfield chemical shift of G19H1′ (4.72 ppm). This situation is also very similar to that described for RNA duplexes with G:A tandem mismatches (Santalucia & Turner, 1993; Ebel et al., 1994). In those cases, NMR

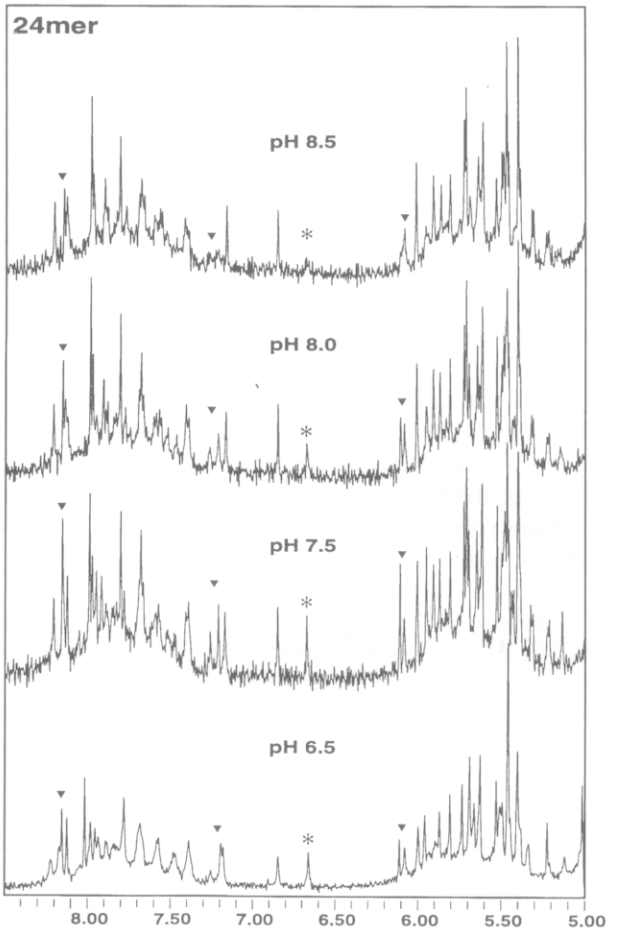

FIGURE 8. Aromatic and anomeric region of 1H NMR of 24mer for pH 6.5–8.5 (10 mM potassium phosphate, 5 mM $MgCl_2$, 30 °C): A5 H2 (*) resonance and other areas of noticeable change (▼) are marked (from left to right: A21H2, G22H8 and G6H8, A5H1′ and A18H1′).

structures have been determined that exhibited strongly twisted amino-paired G:A base pairs and considerable deviations from A-form geometry at the junctions. For both duplexes, the H1′ chemical shift of the 3′-guanosine adjacent to the adenine of the G:A pairs experiences a significant upfield shift ($\delta_{H1'} = 4.32$ ppm [Santalucia & Turner, 1993]). However, it has also been recognized that G:A base pair formation depends upon the flanking sequences. For example, an RNA duplex containing a succession of two G:A/U:A pairings flanked by largely G:C base pairs (Varani et al., 1989) assumed an open structure for the $\begin{matrix}5'\text{G A A U}\\3'\text{A U G A}\end{matrix}$ block; none of the A:U pairs were formed and several base resonances were broadened; however, all puckers were A-form, except the 5′-G, and many NOEs reflected typical A-form patterns. This situation is reminiscent of our 24mer, where the most unexpected result that evidence for the standard A17:U8 base pair was missing. Conceivably, the accommodation of a G:A pair in an A-form helix is associated with structural perturbations that prevent the formation of an adjacent A:U pair. However, one might argue that an A:U pair should form in the case where the G:A pair is not established because there are then more conformational possibilities. Therefore, we can hypothesize that, in the case of the 24mer, the G:A is actually formed at the cost of the adjacent A:U pair. This argument is also based on the observation that the largest structural disruption of A-form geometry is around the G6pG7 and G19pC20 steps, indicated by missing sequential NOEs and the ribose flexibility of C20. Because we have no indications for a structured G:G association, the stabilization of this area in the molecule upon Mg^{2+} uptake suggests that some energetically favorable elements must exist, such as a G:A pair.

NMR structural analysis in light of chemical and enzymatic probing

Enzymatic and chemical probing methods (Jaeger et al., 1993) have been applied recently to 4.5S RNA (Lentzen et al., 1996) in the presence of Mg^{2+}, providing an interesting comparison for our NMR analysis. It was noted that reactivity toward single strand-specific RNases of all internal loop regions, including those in our NMR fragments, was rather low, indicating a compact structure with only few accessible positions. Enzymatic cleavages of the 24mer in the context of 4.5S RNA were observed only in the tetraloop. Interestingly, guanosine-specific RNase T1 yielded the typical, weak cleavage patterns for all guanosines; no cleavage occurred for G15, indicating its involvement in a double-helical fragment, which is in agreement with our NMR analysis.

The 4.5S RNA appeared highly resistant to chemical probes (Lentzen et al., 1996). For the section represented by the 24mer, typical ketoxal modification of guanosines were observed only in the tetraloop; weak effects were also seen for G6 and G7, but not for G19. Although a strong reaction with DMS was seen only for A5, weak hits involved A13, A14, A17, and A21, but not A18. The latter finding agrees with our interpretation, which has A18 involved in a G:A base pair. It was also noted that 4.5S RNA was resistant to modifications by DEPC and CMCT, suggesting that all uracils are somewhat protected and the N7 position of the adenines is not accessible, which would not be compatible with an open, unstructured geometry. However, the strong response of A5 to DMS cannot be rationalized easily by our NMR data, which suggested that A5 is involved in a A^+:C pair. On the other hand, it is important to look at the modification data in light of their most interesting conclusion: the suggestion that 4.5S RNA exhibits a bend largely located around the asymmetric bulge (see Fig. 1). As a consequence, the side of the symmetric bulge with residues C4-A5-G6 is more

accessible than the other. On the other hand, some of the target nitrogen atoms might also be fairly accessible because they are not involved in hydrogen bonds. However, this might be an indication that the bulge structure in the 24mer is somewhat different from that in full, free 4.5S RNA. Another interesting detail of the modification study is the lead cleavage pattern, which usually indicates a highly ordered structural region, often associated with a binding site for divalent cations, such as Mg^{2+}. Strong lead cleavage sites were only observed at the bottom of the asymmetric bulge, and not in the symmetric 24mer bulge, where our data indicate a strong Mg^{2+} effect.

CONCLUSIONS

Two RNA fragments representing portions of the conserved domain IV have been introduced that bind specifically to *ffhM*, the domain of the *E. coli* homologue of SRP54 instrumental for signal sequence recognition. The binding affinity is reduced by an order of magnitude when the asymmetric bulge moiety of domain IV is omitted. Both fragments exhibit a pronounced structural stabilization upon addition of $MgCl_2$. The profile of the 43mer T_m dependence on the Mg^{2+} concentration suggests that the stabilization involves at least one specific binding site for Mg^{2+}. More detailed structure analysis using homonuclear 2D NMR data revealed that Mg^{2+}-specific effects are located in the symmetric bulge, which is present in both 43mer and 24mer constructs. Mg^{2+} seems to stabilize specifically residue A5, which most likely engages in a A^+:C base pair, indicated through the disappearance of the A5H2 resonance at higher pH values. However, the Mg^{2+}-induced stabilization is seen even in the lower part of the top stem, involving a G:A base pair and an A:U pairing, which does not exhibit NOEs typical for either Watson–Crick or Hoogsteen geometries. This suggests that the region exhibiting unusual structural features comprises the

5′-U3	C4	A5	G6	G7	U8	
3′-G22	A21	C20	G19	A18	A17	

segment, which is clearly larger than the secondary structure predicted.

NMR assignments for all base, H1′, and H2′ protons of the 24mer, as well as most imino protons, lead to a preliminary coarse structural model. In the presence of Mg^{2+}, the 24mer assumes a relatively stable compact structure with NOE patterns typical for A-form helices; no indications are seen for syn-conformations, unusual base triplets in the bulge region, or extrahelical nucleotides. Our GGAA tetraloop showed NOEs expected for the structure similar to that of the GCAA tetraloop (Heus & Pardi, 1991), but with some indications for the second guanosine being partially stacked on the adenine base, similar to the loop of the recent ribozyme crystal structure (Pley et al., 1994). The largest disruption of A-form helicity is associated with the two guanosine residues in the symmetric bulge. Their imino protons do not engage in hydrogen bonding, but that does not preclude pairings involving amino groups.

Spectral similarities between 24mer and 43mer in the upfield aromatic region and the region of the imino protons not protected from exchange with solvent suggest that the symmetric bulge in both fragments assumes a similar structure and has a similar Mg^{2+} dependence. This suggests that the asymmetric bulge cannot greatly influence structure and stability of the symmetric bulge. In general, the pH and Mg^{2+} dependence of the 24mer structure might indicate the malleability of the symmetric bulge, which could play an important role in its interaction with SRP54. Because *ffhM* binding is not adversely affected for Mg^{2+}-free conditions, it is clear that even a flexible symmetric bulge is recognized by *ffhM*, and Mg^{2+}-induced structural features are not relevant for the process. This also suggests that the structure for the bound form might deviate substantially from either free RNA structure.

A more detailed structural study will require additional proton assignments, especially for the exchangeable protons, requiring heteronuclear NMR methods. We expect this information to come from our NMR work with the double-labeled SRP 43mer fragment, whose solution structure determination is in progress.

MATERIALS AND METHODS

RNA synthesis and purification

The SRP 43mer was synthesized by in vitro transcription using T7 RNA polymerase on a synthetic DNA template according to the method of Milligan et al. (1987). The transcription reaction was optimized to yield 10 O.D./mL reaction mixture using final conditions of 0.4 M Tris-HCl, pH 8.1, 36 mM $MgCl_2$, 50 mM dithiothreitol, 10 mM spermidine, 6 mM each ATP, CTP, GTP, and UTP, 0.1 % Triton X-100, 800 nM DNA template, and 5 μg/mL T7 RNA polymerase. The mixture was incubated at 37 °C for 4 h in a total volume of 25 mL. After precipitation with ethanol and centrifugation, the RNA-containing pellet was dissolved in 8 mL 7-M urea and purified on five 20% polyacrylamide/7-M urea gels (43 × 35 × 0.15 cm). The bands of the full-length RNA and the "$n + 1$" product were excised, electroeluted, precipitated with ethanol, and finally dialyzed against a cascade of buffers [10 mM KP, 5 mM EDTA, 100 mM NaCl; 10 mM KP, 0.1 mM EDTA, 100 mM NaCl; 10 mM KP, 50 mM NaCl; water] for 24 h each at 4 °C, pH 6.4, using a membrane with a 3,500 molecular weight cut-off. The SRP 24mer was synthesized on an ABI synthesizer, model 394, using phosphoramidite coupling chemistry with some recent improvements in deprotection and precipitation steps (Sproat et al., 1995). The crude material (800 $O.D._{260}$) was gel-purified analogous to the procedure described for the 43mer, yielding 120 $O.D._{260}$.

Expression and purification of the M-domain of the *E. coli* SRP 54 homologue

ffhM was overexpressed from *E. coli* as described by R.J. Keenan, D.M. Freymann, R. Stroud, and P. Walter (in prep.). Briefly, 3 L of cells were lysed and *ffhM* was purified using a combination of ion exchange and heparin affinity chromatography. Typical yields are ca. 4 mg/L, with a purity of ca. 95%.

3′-Labeling of RNA

RNA fragments were labeled at the 3′-end with [5′-32P]pCp (England et al., 1980) using T4 RNA ligase (News England Biolabs). Labeled RNAs were purified with 7 M urea–15% PAGE, and extracted by crush-and-soak methods followed by ethanol precipitation.

Nitrocellulose binding assay

Reaction mixtures (20 μL) containing between 20 and 100 nM 3′-labeled RNAs and varying concentrations of the M-domain of *E. coli* SRP54 homologue (1–2,000 nM) in binding buffer (10 mM HEPES, 100 mM NaCl, 1.5 mM DTT, 5 mM $MgCl_2$, 0.01% Nikkol, pH 7.0) were incubated for 20 min on ice and assayed by nitrocellulose filtration at least three times for each set. Schleicher & Schuell 0.45-μm filters were presoaked at least 10 min at room temperature and washed with 5 × 2-mL 25 mM potassium phosphate, pH 7.0, after application of the reaction mixture. Radiolabeled RNA was quantified and normalized to the total RNA present. With saturation of the M-domain, 80–95% of the radiolabeled RNAs were trapped. Because the exact concentration of the labeled RNA is difficult to determine, we obtained the apparent dissociation constant (K_D) by nonlinear least-squares fit of the normalized binding data to a generalized binding equation (Segel, 1991), where K_D and RNA concentration were adjustable parameters. In some cases, the latter parameter was fixed at 100 mM when the fit produced unreasonably large RNA concentrations. Analysis was performed with the program MacCurveFit (Raner, 1995). For competition binding assays, a mixture of *ffhM* (500 nM), radiolabeled RNA (50 nM), and various amounts of cold RNA competitor (10–1,000 nM) were incubated together for 20 min at room temperature.

NMR sample preparation

The SRP RNA fragments were lyophilized several times from D_2O for analysis of nonexchangeable protons. For the SRP 24mer, the lyophilized powder was dissolved in 1 mL of buffered D_2O with TSP as internal standard. The sample was annealed immediately prior to use by heating at 75 °C for 10 min and snap-cooling on ice for 30 min. To minimize the formation of dimeric species, Mg^{2+} salts were added after annealing, immediately prior to conducting NMR experiments. Note that the SRP 24mer was subjected to the complete procedure of dialysis, lyophilization, snap-cooling, and addition of Mg^{2+} before each 2D NMR experiment. Final conditions for the 24mer were 0.25 mM RNA, 5 mM $MgCl_2$, 10 mM potassium phosphate, and pH 6.5, unless noted otherwise. For analysis of exchangeable protons, the sample was lyophilized and dissolved in 9:1 H_2O:D_2O containing TSP and 10 mM potassium phosphate, pH 6.4. The same conditions were used for the SRP 43mer, except that the RNA concentration could be kept much higher (1.8 mM in 250 μL). For the pH- and Mg^{2+}-titration experiments, a concentrated stock solution of NaOD, DCl, or $MgCl_2$ in D_2O was added directly into the NMR tube; thus, all Mg^{2+} concentrations represent total concentrations.

Thermodynamic measurements

Thermal denaturation profiles were measured on a Cary 3E UV-visible spectrophotometer equipped with temperature controller, at a heating rate of 0.5 or 1 °C/min, with detection at 260 nm. Data were collected on 1-mL samples for various conditions over the temperature range 15–97 °C. In general, stock solutions of the RNAs were diluted into buffered solvent (10 mM potassium cacodylate or MOPS, pH 6.5), degassed, and annealed. All other salts were added immediately prior to the melting experiment, after the annealing step, as described for the NMR sample.

Gel filtration HPLC was performed on a Superose 12 column, running at 0.5 mL/min at a pressure of ~28 bar with detection at 260 nm. Samples (1–5 mg/mL) were prepared in the running buffers at pH 6.4, heated to 75 °C for 7 min, then either snap-cooled on ice or cooled slowly overnight.

NMR experiments

^1H NMR experiments were acquired at 600 MHz on a Varian Unityplus spectrometer or at 500 MHz on a General Electric GN500. All 2D NOE spectra (τ_m = 50, 150, and 400 ms) in D_2O were acquired in the hypercomplex mode (States et al., 1982) at 25 or 30 °C, using a spectral width of 5,999 Hz in both dimensions with the carrier frequency set to the HDO resonance frequency. Four-hundred t_1 values were recorded for each fid. Thirty-two scans with a repetition time of 2.0 s were recorded for each t_1 increment with 2K data points in f_2. Double-quantum filtered COSY spectra were acquired under the same conditions. TOCSY experiments were run with MLEV-17 mixing and cycling (Bax & Davis, 1985) with mixing times of 30 and 75 ms.

All 2D NOE experiments in H_2O were collected at 10 °C using the SSnoesy pulse sequence (Smallcombe, 1993) with a spectral width of 12,000 Hz using a symmetrically shifted S-pulse with pulse width of 88.8 μs for water suppression. Excitation maximum occurs at ±7,576 Hz from the carrier frequency. Mixing times were 150 and 400 ms. Acquisition parameters were as described above except that 64 or 128 scans were used per fid.

1D NMR experiments in H_2O were acquired with a $1\bar{3}3\bar{1}$ pulse (Hore, 1983) for solvent suppression on a GE GN-500 MHz spectrometer with the maximum excitation set to 10.5 ppm. Longitudinal relaxation experiments were performed using the inversion-recovery method.

2D data sets were transferred to a SUN SPARCstation 2 and were processed using Striker and Sparky (Kneller, 1992). A Gaussian window function was used for resolution enhancement (Gaussian multiplier of 0.15 and line broadening of −7.0) in both dimensions for TOCSY and SSNOESY spectra. For DQF-COSY, the data were apodized with a 30–45°

shifted sinebell function. NOESY spectra were processed with a 60° shifted sinebell function. Prior to Fourier transformation, the fids were zero-filled to give a final 2k × 2k data set.

ACKNOWLEDGMENTS

We thank Dr. James Kealey for help with the binding assays. This research was supported by NIH grant GM39247 to T.L.J. and a UC Academic Senate Research Grant as well as a NSF grant (MCB-9513214) to U.S. We gratefully acknowledge the UCSF Computer Graphics laboratory supported by NIH grant RR01081.

Received August 8, 1996; returned for revision September 17, 1996; revised manuscript received October 7, 1996

REFERENCES

Althoff S, Selinger D, Wise JA. 1994. Molecular evolution of SRP cycle components: Functional implications. *Nucleic Acids Res 22*: 1933–1947.

Bax A, Davis DG. 1985. MLEV-17-based two-dimensional homonuclear transfer spectroscopy. *J Magn Reson 65*:355–372.

Bernstein HD, Poritz MA, Strub K, Hoben PJ, Brenner S, Walter P. 1989. Model for signal sequence recognition from amino-acid sequence of 54 kD subunit of signal recognition particle. *Nature 340*:482–486.

Bernstein HD, Zopf D, Freymann DM, Walter P. 1993. Functional substitution of the signal recognition particle 54-kDa subunit by its *Escherichia coli* homologue. *Proc Natl Acad Sci USA 90*:5229–5233.

Borer PN, Lin Y, Wang S, Roggenbuck MW, Gott JM, Uhlenbeck OC, Pelczer I. 1995. Proton NMR and structural features of a 24-nucleotide RNA hairpin. *Biochemistry 34*:6488–6503.

Ebel S, Brown T, Lane AN. 1994. Thermodynamic stability and solution conformation of tandem G:A mismatches in RNA and RNA–DNA hybrid duplexes. *Eur J Biochem 220*:703–715.

England TE, Bruce AG, Uhlenbeck OC. 1980. Specific labeling of 3′ termini of RNA with T4 RNA ligase. *Methods Enzymol 65*:65–74.

Hauser S, Bacher G, Dobberstein B, Lütcke H. 1995. A complex of the signal sequence binding protein and the SRP RNA promotes translocation of nascent proteins. *EMBO J 14*:5485–5493.

Heus HA, Pardi A. 1991. Structural features that give rise to the unusual stability of RNA hairpins containing GNRA loops. *Science 253*:191–194.

High S, Flint N, Dobberstein B. 1991. Requirement for the membrane insertion of signal-anchor type proteins. *J Cell Biol 113*:25–34.

Hore PJ. 1983. Solvent suppression in fourier transform nuclear magnetic resonance. *J Magn Reson 55*:283–300.

Jaeger JA, Santalucia J, Tinoco I. 1993. Determination of RNA structure and thermodynamics. *Annu Rev Biochem 62*:255–287.

Jones OW, Berg P. 1966. Studies on the binding of RNA polymerase to polynucleotides. *J Mol Biol 22*:199–206.

Kennedy MA, Nuutero ST, Davis JT, Drobny GP, Reid BR. 1993. Mobility at the TpA cleavage site in the T_3A_3-containing AhaIII and PmeI restriction sequences. *Biochemistry 32*:8022–8035.

Kneller DG. 1992. *Sparky, NMR display and processing program*. San Francisco, California: University of California.

Kurita K, Honda K, Suzuma S, Takamatsu H, Nakamura K, Yamane K. 1996. Identification of a region of bacillus subtilis *ffh*, a homologue of mammalian SRP54 protein, that is essential for binding to small cytoplasmic RNA. *J Biol Chem 271*:13140–13146.

Laing LG, Gluick TC, Draper DE. 1994. Stabilization of RNA structure by Mg ions—Specific and non-specific effects. *J Mol Biol 237*:577–587.

Larsen N, Zwieb C. 1993. The signal recognition particle database (SRPDB). *Nucleic Acids Res 21*:3019–3020.

Legault P, Pardi A. 1994. In situ probing of adenine protonation in RNA by 13C-NMR. *J Am Chem Soc 116*:8390–8391.

Lentzen G, Dobberstein B, Wintermeyer W. 1994. Formation of SRP-like particle induces a conformational change in *E. coli* 4.5S RNA. *FEBS Lett 348*:233–238.

Lentzen G, Moine H, Ehresmann B, Wintermeyer W. 1996. Structure of 4.5S RNA in the signal recognition particle of *Escherichia coli* as studied by enzymatic and chemical probing. *RNA 2*:244–253.

Lingbeck J, Kubinec MG, Miller J, Reid BR, Drobny GP, Kennedy MA. 1996. Effect of adenine methylation on the structure and dynamics of TpA steps in DNA—NMR structure determination of $[d(CGAGGTTTAAACCTCG)]_2$ and its A9-methylated derivative at 750 MHz. *Biochemistry 35*:719–734.

Lütcke H. 1995. Signal recognition particle (SRP), a ubiquitous initiator of protein translocation. *Eur J Biochem 228*:531–550.

Milligan JF, Groebe DR, Wilherell GW, Uhlenbeck OC. 1987. Oligoribonucleotide synthesis using T7 RNA polymerase and synthetic DNA templates. *Nucleic Acids Res 15*:8783–8798.

Nikonowicz EP, Pardi A. 1993. An efficient procedure for assignment of the proton, carbon and nitrogen resonances in C-13/N-15 labeled nucleic acids. *J Mol Biol 232*:1141–1156.

Pardi A. 1995. Multidimensional heteronuclear NMR experiments for structure determination of isotopically labeled RNA. *Methods Enzymol 261*:350–382.

Pley HW, Flaherty KM, Mckay DB. 1994. Model for an RNA tertiary interaction front the structure of an intermolecular complex between a GAAA tetraloop and an RNA helix. *Nature 372*:111–113.

Poritz MA, Strub K, Walter P. 1988. Human SRP RNA and *E. coli* 4.5S RNA contain a highly homologous structural domain. *Cell 55*:4–6.

Puglisi JD, Tinoco IJ. 1989. Absorbance melting curves of RNA. *Methods Enzymol 180*:304–325.

Puglisi JD, Wyatt JR. 1995. Biochemical and NMR studies of RNA conformation with an emphasis on RNA pseudoknots. *Methods Enzymol 261*:323–349.

Puglisi JD, Wyatt JR, Tinoco I Jr. 1990. Solution conformation of an RNA hairpin loop. *Biochemistry 29*:4215–4226.

Raner K. 1995. *MacCurveFit*. Weaverly, Australia: Kevin Raner Software.

Römisch K, Webb J, Herz J, Prehn S, Frank R, Vingron M, Dobberstein B. 1989. Homology of the 54K protein of signal recognition particle, docking protein, and two *E. coli* proteins with putative GTP-binding domains. *Nature 340*:478–482.

Römisch K, Webb J, Lingelbach K, Gausepohl H, Dobberstein B. 1990. The 54-kD protein of signal recognition particle contains a methionine-rich RNA binding domain. *J Cell Biol 111*:1793–1802.

Santalucia J, Turner D. 1993. Structure of $r(GGCGAGCC)_2$ in solution from NMR and restrained MD. *Biochemistry 32*:12612–12623.

Schmitz U, Sethson I, Egan WM, James TL. 1992. Solution structure of a DNA octamer containing the Pribnow box via restrained molecular dynamics simulation with distance and torsion angle constraints derived from 2D NMR spectral fitting. *J Mol Biol 227*: 510–531.

Segel A. 1991. *Biological kinetics*. Cambridge: Cambridge University Press.

Shen LX, Cai Z, Tinoco I. 1995. RNA structure at high resolution. *FASEB J 9*:1023–1033.

Smallcombe SH. 1993. Solvent suppression with symmetrically-shifted pulses. *J Am Chem Soc 115*:4776–4785.

Sproat B, Colonna F, Mullah B, Tsou D, Andrus A, Hampel A, Vinayak R. 1995. An efficient method for the isolation and purification of oligoribonucleotides. *Nucleosides and Nucleotides 14*:255–273.

States DJ, Haberkorn RA, Ruben DJ. 1982. A two-dimensional nuclear Overhauser experiment with pure absorption phase in four quadrants. *J Magn Reson 48*:286–292.

Varani G, Tinoco I. 1991. RNA structure and NMR spectroscopy. *Q Rev Biophys 24*:479–532.

Varani G, Wimberly B, Tinoco IJ. 1989. Conformation and dynamics of an RNA internal loop. *Biochemistry 28*:7760–72.

Wagner G. 1993. Prospects for NMR of large proteins. *J Biomol NMR 3*:375–385.

Walter P, Johnson AE. 1994. Signal sequence recognition and protein targeting to the endoplasmic reticulum membrane. *Annu Rev Cell Biol 10*:87–119.

Wijmenga SS, Mooren MMW, Hilbers CW. 1994. NMR of nucleic acids: from spectrum to structure. In: Roberts GCK, ed. *NMR of Macromolecules 134*. Oxford: Oxford University Press. pp 217–288.

Woese CR, Winker S, Gutell RR. 1990. Architecture of ribosomal RNA: Constraints on the sequence of "tetra-loops." *Proc Natl Acad Sci USA 87*:8467–8471.

Wüthrich K. 1986. *NMR of proteins and nucleic acids*. New York: Wiley.

Yao L, James TL, Kealey J, Santi DV, Schmitz U. 1996. The dynamic NMR structure of the TΨ-loop: Implications for tRNA methylation. *J Biomol NMR*. Forthcoming.

Zopf D, Bernstein HD, Johnson AE, Walter P. 1990. The methionine-rich domain of the 54 kD protein subunit of the signal recognition particle contains an RNA binding site and can be crosslinked to a signal sequence. *EMBO J 9*:4511–4517.

Zopf D, Bernstein HD, Walter P. 1993. GTPase domain of the 54-kD subunit of the mammalian signal recognition particle is required for protein translocation but not for signal sequence binding. *J Cell Biol 120*:1113–1121.